Supporting Information

Molecular Orientation-Steric Hindrance Tradeoff of Cyclohexylammonium Passivators for High-Performance Perovskite Solar Cells

Shuang Gao,†[a] Zehuan Jia,†[b] Shantao Zhang,[a] Xinyu Li,[a] Dehan Li,[a] Yue Zhang,[a] Tianao Hou,[c] Rongyao Lv,[a] Zhimin Fang,*[d] Wenjing Chen,[e] Tao Chen,[a] Zhengguo Xiao,[e] Junfa Zhu,[f] Xiaojun Wu,*[b] Xu Pan*[g] and Shangfeng Yang*[a]

[a] State Key Laboratory of Precision and Intelligent Chemistry, Collaborative Innovation Center of Chemistry for Energy Materials (iChEM), Anhui Laboratory of Advanced Photon Science and Technology, Department of Materials Science and Engineering, University of Science and Technology of China, Hefei 230026, China. E-mail: sfyang@ustc.edu.cn

[b] Hefei National Laboratory for Physical Sciences at the Microscale, Synergetic Innovation of Quantum Information and Quantum Technology, CAS Center for Excellence in Nanoscience, and School of Chemistry and Materials Sciences, University of Science and Technology of China, Hefei 230026, China. E-mail: xjwu@ustc.edu.cn

[c] Hefei National Laboratory, University of Science and Technology of China, Hefei 230088, China

[d] Institute of Technology for Carbon Neutralization, Yangzhou University, Yangzhou 225127, China. E-mail: fangzm@yzu.edu.cn

[e] CAS Key Laboratory of Strongly-coupled Quantum Matter Physics, Department of Physics, University of Science and Technology of China, Hefei 230026, China

[f] National Synchrotron Radiation Laboratory, Department of Chemical Physics and Key Laboratory of Surface and Interface Chemistry and Energy Catalysis of Anhui, Higher Education Institutes, University of Science and Technology of China, Hefei 230026, China

[g] Key Laboratory of Photovoltaic and Energy Conservation Material, Institute of Solid-State Physics (ISSP), Hefei Institutes of Physical Science (HIPS), Chinese Academy of Sciences, Hefei 230031, China. E-mail: xpan@rntek.cas.cn

*Corresponding authors.

†These authors contributed equally to this work.

Experimental methods

Materials

All chemicals were used as received without further purification, including urea (Sigma-Aldrich, ≥99%), hydrochloric acid (HCl, 37 wt. % in water, Sinopharm Chemical Reagent Co., Ltd), thioglycolic acid (Sigma-Aldrich, 98%), $SnCl_2 \cdot 2H_2O$ (Aladdin, ≥99.99%), KCl (Aladdin, ≥99.99%), PbI_2 (TCI, 99.99%) , methylammonium chlorine (MACl, Xi'an Polymer Light Technology Corporation), formamidinium iodide (FAI, Great Cell Solar), Cyclohexylammonium iodide (Aladdin, ≥98%), Cyclohexylmethylammonium iodide (Aladdin, ≥98%), Cyclohexylethylammonium iodide, and Cyclohexylpropylammonium iodide were obtained through the one-step hydroiodic acid acidification of the corresponding amine molecules (Aladdin, ≥98%), 2,2',7,7'-Tetrakis[N, N-di(4-methoxyphenyl)amino]-9,9'-spirobifluorene (spiro-OMeTAD, Advanced Election Technology Co., Ltd), 4-tert-Butylpyridine (t-BP, Adamas), li-bis(trifluoromethanesulfonyl)imide (Li-TFSI, Sigma-Aldrich), Tris(2-(1H -pyrazol-1-yl)-4-tert-butylpyridine)-cobalt(III)Tris(bis(trifluoromethylsulfonyl)imide)) salt (Co(III) TFSI, GreatCell Solar), PTAA (Xi'an Polymer Light Technology Corporation), and 4-isopropyl-40-methyldiphenyliodonium Tetrakis(pentafluorophenyl)borate (TPFB, TCI, 98%). Dimethylformamide (DMF), dimethyl sulfoxide (DMSO), chlorobenzene (CB), and acetonitrile (ACN) were all purchased from Sigma-Aldrich. Isopropyl alcohol (IPA), chloroform, and diethyl ether were all purchased from Sinopharm Chemical Reagent Co., Ltd.

Device Fabrication

The fluorine-doped tin oxide (FTO) glass substrates (1.5 × 1.5 cm^2, Suzhou ShangYang Solar Technology Co., Ltd.) were cleaned by sequential ultrasonic treatment in detergent, deionized water, acetone, and IPA for 15 min each. Then, the substrates were dried by nitrogen flow. Before fabricating the SnO_2 layer, the substrates were treated

with UV-ozone for 30 min. The SnO_2 layer was fabricated by the chemical bath deposition (CBD) method according to our previous work.[1] Briefly, the solution was prepared by dissolving 1250 mg of urea in 100 mL deionized water, followed by adding 1250 μL HCl and 25 μL of thioglycolic acid. Finally, 275 mg $SnCl_2 \cdot 2H_2O$ was added to the solution followed by stirring for 2 min. Then, the FTO substrates, which were taped with a Kapton tape on the edge to prevent deposition of SnO_2, were vertically placed inside the glassware that contained about 100 mL of the solution. The glassware was placed inside a water bath set to 94 °C. After 4 hrs reaction, the FTO/SnO_2 substrates were removed from the glassware and cleaned via sonication with deionized water and IPA for 5 min each and then dried by nitrogen flow. The FTO/SnO_2 substrates were annealed in an ambient environment (relative humidity: ~25%) at 170 °C for 1 hr. After cooling to room temperature, the substrates were treated by UV-ozone for 15 min, followed by spin-coating 10 mM KCl in deionized water at 3000 rpm for 30 sec and annealing at 100 °C for 10 min. Before the perovskite deposition, the KCl-modified FTO/SnO_2 substrates were treated by UV-ozone for 15 min and then pumped inside a nitrogen glovebox.

The perovskite precursor solution was prepared by mixing 1.53 M PbI_2, 1.4 M FAI, 0.5 M MACl in mixed solvents (DMF: DMSO=8:1, v: v). To simplify, the perovskite was abbreviated as $FAPbI_3$. The perovskite precursor solution was deposited via spin-coating at 1000 rpm for 10 sec, and 5000 rpm for 30 sec, both with the ramp of 2000 rpm/sec. 700 μL of diethyl ether solution was deposited onto the substrate as 20 sec left of the procedure. Subsequently, the FTO/SnO_2/perovskite substrate was annealed at 120 °C for 1 hr. After the substrate was cooled to room temperature, four types of cyclohexylammonium salt passivators (10 mM) in IPA solution was deposited onto the perovskite layer at 4000 rpm for 30 sec and annealed at 100 °C for 5 min. The hole transporting layer (HTL) solution, which contains 100 mg spiro-OMeTAD, 39 μL t-BP, 10 μL Co(III) TFSI solution (0.25 M in ACN), 23 μL Li-TFSI solution (1.8 M in ACN), and 1100 μL CB, was spin-coated onto the treated perovskite film at 3000 rpm for 30 sec with the ramp of 3000 rpm/sec. For the dry air treatment (DAT) method to

oxidize spiro-OMeTAD, the as-prepared spiro-OMeTAD film was stored in a vacuum dry box (temperature: 55°C, relative humidity: 15%) for 5 hrs. Subsequently, 80 nm silver was deposited via a shadow mask at a pressure of about 2×10^{-4} Pa in a vacuum chamber. The concentration of PTAA was 30 mg mL1 in toluene, and the weight ratio of PTAA/TPFB was 10:1. The PTAA was deposited on top of perovskite layer at a spin rate of 2,000 rpm for 30 s. The deposition rate of Ag was maintained at 0.1 Å/sec for the first 5 nm and then changed to 0.2 Å/sec to deposit 6-10 nm, finally the rate changed to 0.4 Å/sec and maintained until the end of the deposition process. The device size area was 0.1369 cm^2 (0.37 × 0.37 cm^2). When measuring, a 0.0905 cm^2 non-reflective metal mask aperture was used to define the accurate active area of the devices.

Characterization

The current density–voltage (*J–V*) characterizations were measured by a Keithley 2400 source measurement unit under simulated AM 1.5 irradiation (100 mW cm^{-2}) with a standard xenon-lamp-based solar simulator (Oriel Sol 3A, USA), which was calibrated with a monocrystalline silicon reference cell (Oriel P/N 91150 V, with KG-5 visible color filter) calibrated by the National Renewable Energy Laboratory (NREL). The active device area during the measurements was 0.0905 cm^2 as defined by a metal mask. All *J-V* measurements were performed under AM 1.5G illumination, with a bias voltage range from -0.1 V to 1.25 V, 100 measurement points, a step delay of 0.1 s, and a scan rate of 0.01 V/s. The external quantum efficiency (EQE) measurements were carried out on an ORIEL Intelligent Quantum Efficiency (IQE) 200TM Measurement system established with a tunable light source. Transient photovoltage (TPV) measurements were carried out with a system excited by a 520 nm pulse laser. Contact angles were performed on an Attension Theta Optical tensiometer (Biolin Scienfitic, Sweden). Scanning electron microscopy (SEM) measurements were attained via a field-emission scanning electron microscope (FEI Apero). The steady state PL spectra was recorded by employing an Edinburgh Instruments FLS920 fluorescence spectrometer with an excitation wavelength of 500 nm. PLQY data were measured using a Horiba Fluorolog-

3 system with a petite integrating sphere. The excitation wavelength was 460 nm, which was provided by a semiconductor laser (DL-405-100-T, Raymount Optronics). Time-resolved PL spectra were measured via the time-correlated single-photon counting method with a PicoQuant Gmbh Solea Supercontinuum Laser. A picosecond pulsed diode laser at 543 nm with a pulse width of 104 ps was used as the excitation source. The X-ray diffraction (XRD) patterns were obtained on a Rigaku SmartLab X-ray diffractometer with Cu-Kα radiation (0.154 nm). Ultraviolet-visible (UV-vis) absorption spectroscopy was recorded on a UV–vis–NIR 3600 spectrometer (Shimadzu, Japan). The ultrafast transient absorption (TA) measurements were performed on a pump-probe system (Helios, Ultrafast System) with the maximum time delay of ~8 ns using a motorized optical delay line under ambient conditions. The pump pulses at 400 nm (~20 μW average power at the sample) were delivered by an ultrafast optical parametric amplifier (Opera Solo) excited by a regenerative amplifier (Coherent Astrella, 800 nm, 35 fs, 5 mJ, 1 kHz), seeded with a mode-locked Ti: sapphire oscillator (Coherent Vitara, 800 nm, 80 MHz) and pumped with a LBO laser (Coherent Evolution-50C, 1 kHz system). The X-ray photoelectron spectroscopy (XPS) measurements and ultraviolet photoelectron spectroscopy (UPS) experiments were performed at the beamline BL11U in the National Synchrotron Radiation Laboratory (NSRL), Hefei. Electrochemical impedance spectroscopy (EIS) was performed in dark using an electrochemical workstation (Autolab 320, Metrohm, Switzerland) with a frequency range from 1 Hz to 1 MHz under 1.0 V. AC 20 mV perturbation was applied with a frequency from 1 MHz to 1 Hz. The obtained impedance spectra were fitted with ZView software (v2.8b, Scribner Associates, USA).

DFT simulations

First-principles calculations based on Density Functional Theory (DFT) were performed using the Vienna Ab-initio Simulation Package (VASP).[1] The interactions between core and valence electrons were described using the projector-augmented wave (PAW) method,[2,3] while the exchange-correlation effects were treated within the

framework of the generalized gradient approximation (GGA) as formulated by Perdew-Burke- Ernzerhof (PBE).[4] To account for dispersive interactions, the zero-damping DFT-D3 method of Grimme was employed.[5] The plane-wave basis set was truncated at a cutoff energy of 450 eV. Convergence criteria for total energy and atomic forces were set to 1×10^{-5} eV/atom and 0.05 eV/Å, respectively. To evaluate the energy changes associated with molecules adsorption on the surface regions, slab models were constructed along the *c*-axis direction, incorporating a vacuum layer larger than 15 Å to eliminate interactions between periodic images. The bottom three layers were fixed during the geometry optimization for slab models. In slab calculations (2×2×1 supercell), a 2 × 2 × 1 grid was applied for structural optimization and self-consistent energy calculations.The binding energies (E_b) of molecules in different phases were calculated as:

$$E_b = E_{complex} - E_{pure} - E_{mole}$$

where the $E_{complex}$ and E_{pure} are the energies of different phases with and without molecules, the E_{mole} is the energy of isolated molecules.

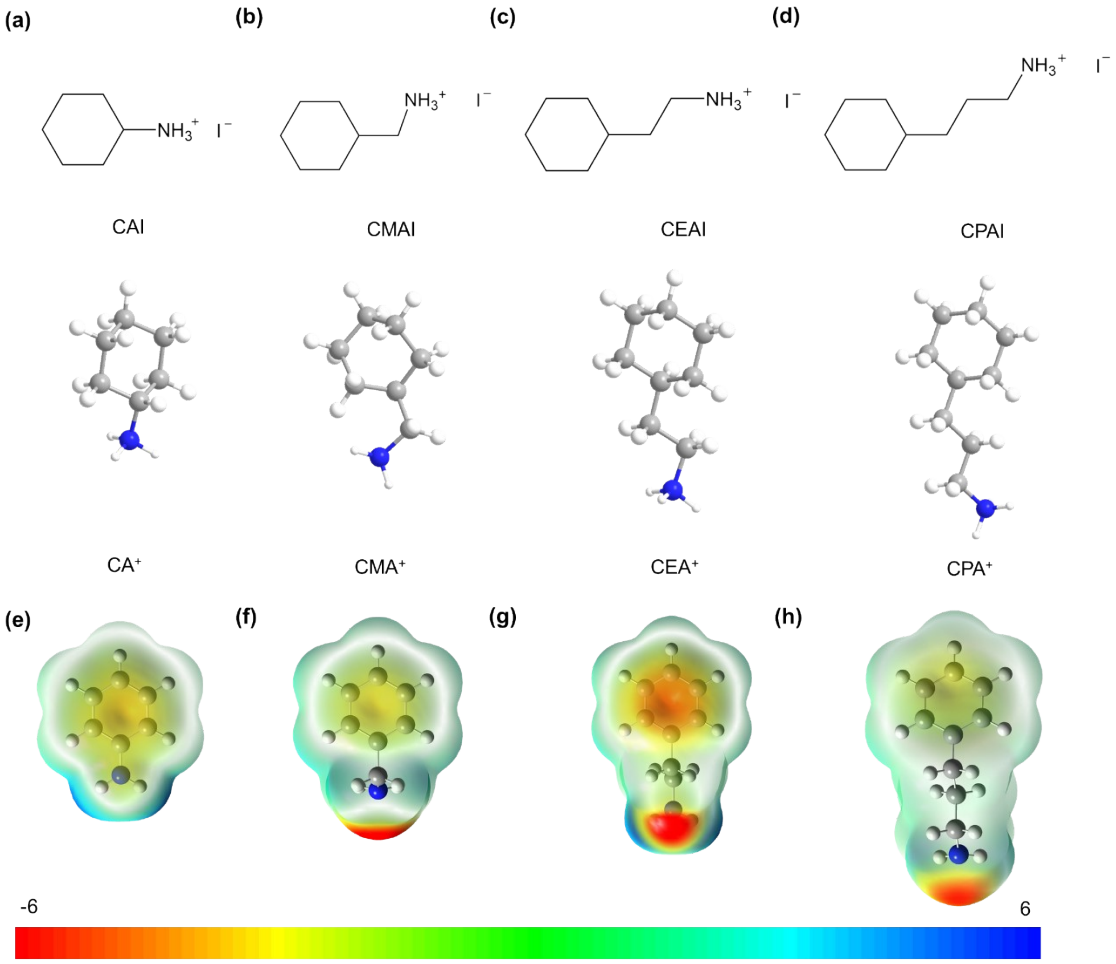

Fig. S1 The molecular structure diagram and electrostatic surface potential (ESP) of (a, e) Cyclohexylammonium iodide (CAI), (b, f) Cyclohexylmethylammonium iodide (CMAI), (c, g) Cyclohexylethylammonium iodide (CEAI), and (d, h) Cyclohexylpropylammonium iodide (CPAI).

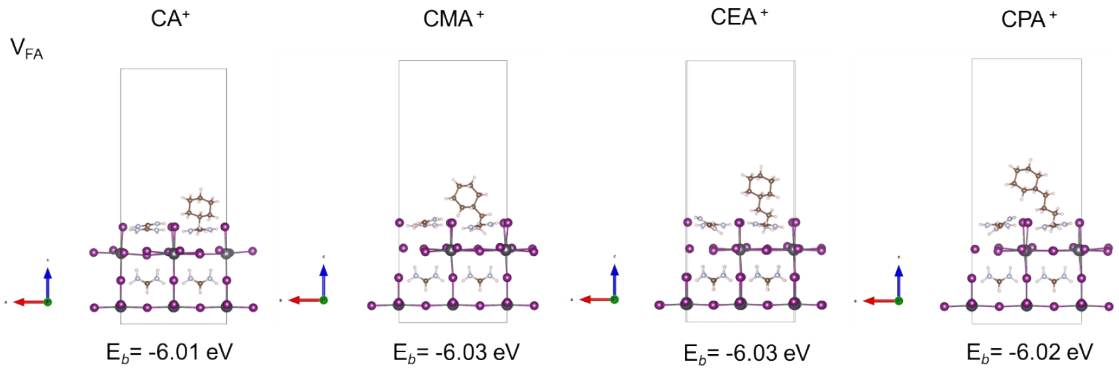

Fig. S2 Side views of the CA^+, CMA^+, CEA^+, and CPA^+ adsorbed on perovskite surfaces with formamidinium (FA) vacancy (V_{FA}).

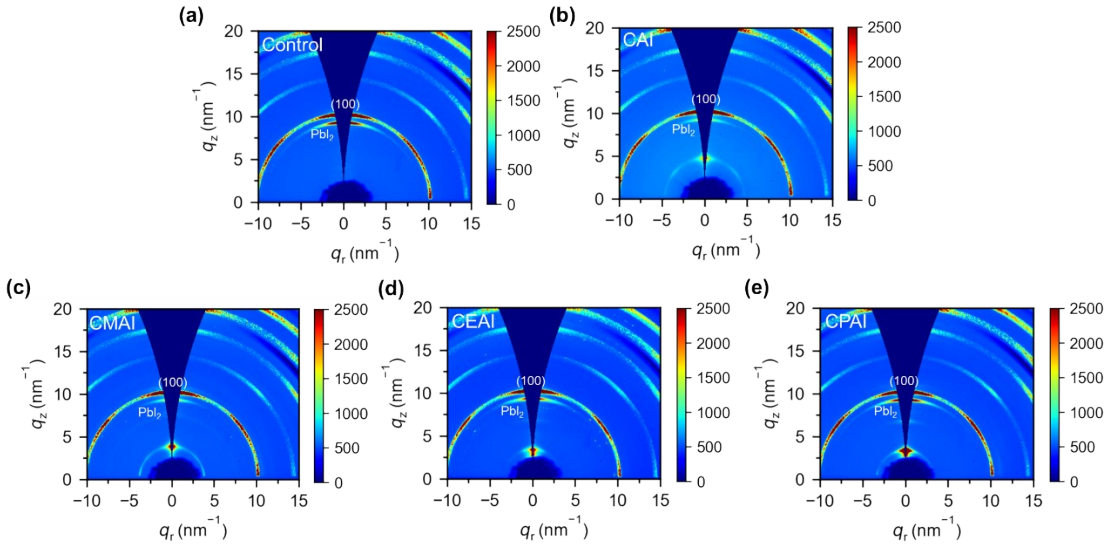

Fig. S3 GIXRD patterns of the control and passivated perovskite films (Excessive concentration: 30 mM).

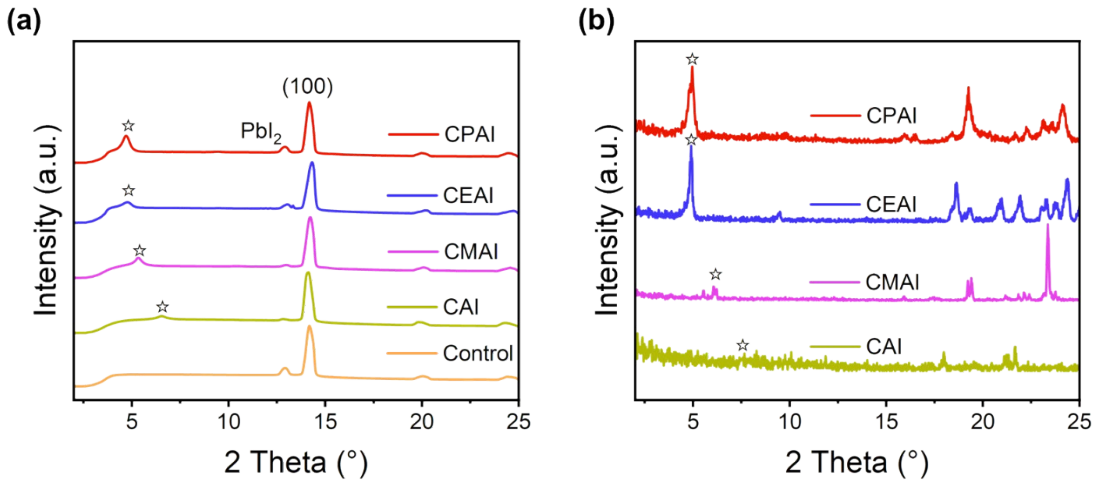

Fig. S4 (a) Radially integrated curves of the control and passivated perovskite films extract from Fig. X1. (b) XRD patterns of different passivation agent powders.

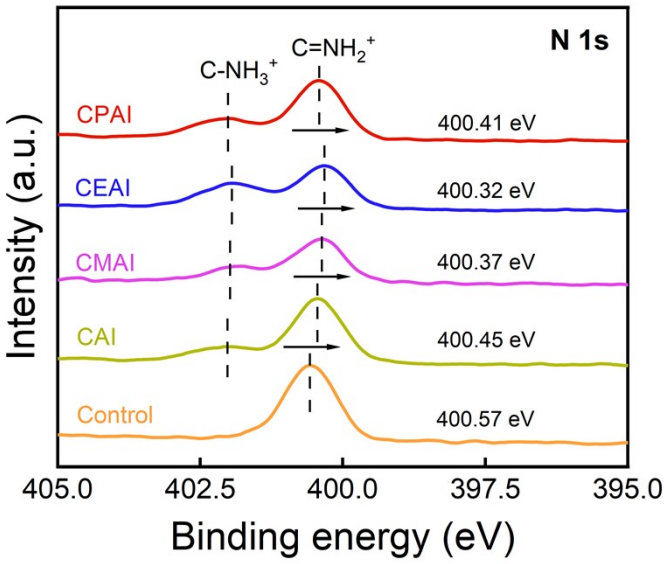

Fig. S5 XPS spectra of N 1s.

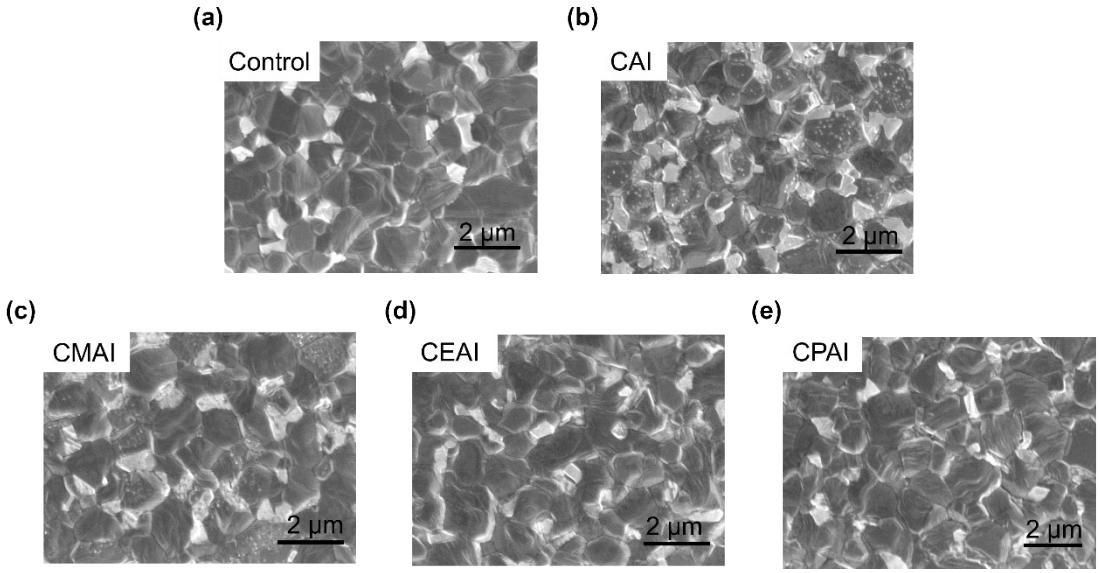

Fig. S6 Top-view SEM images of $FAPbI_3$ perovskite films. (a) Control film. Films modified with cyclohexylammonium salts: (b) CAI, (c) CMAI, (d) CEAI, and (e) CPAI.

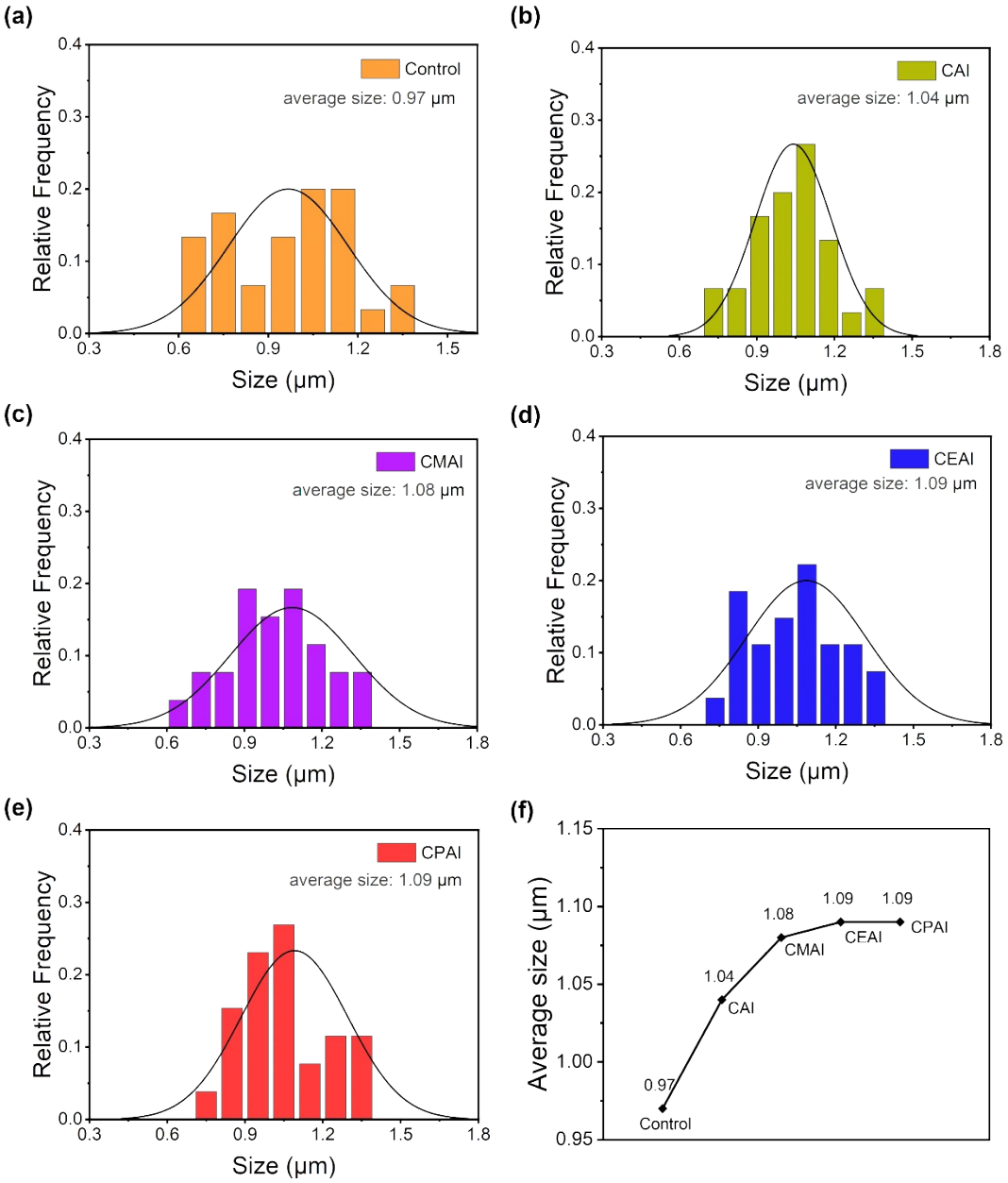

Fig. S7 The corresponding grain size statistics extracted from the top-view SEM images: (a) control film, (b) CAI treatment, (c) CMAI treatment, (d) CEAI treatment, (e) CPAI treatment. (f) Average grain size the control and passivated perovskite films.

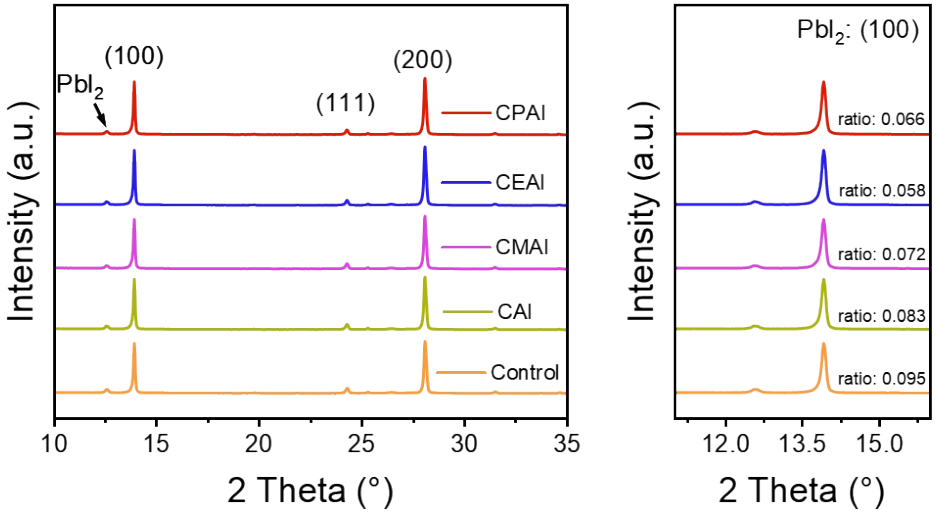

Fig. S8 XRD patterns of the control and passivated perovskite films.

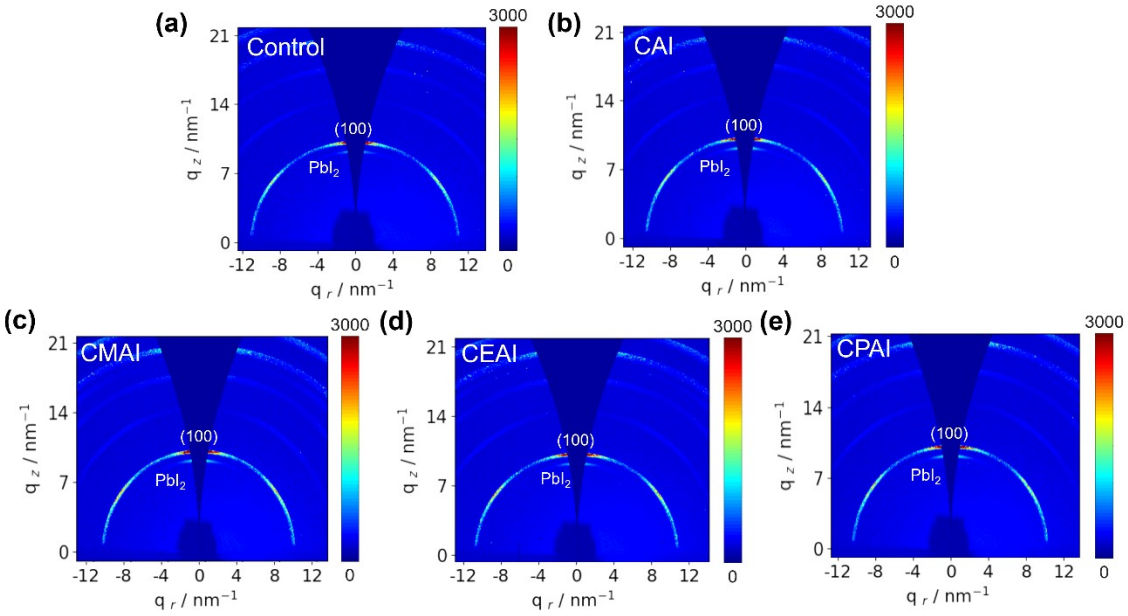

Fig. S9 GIXRD patterns of the control and passivated perovskite films.

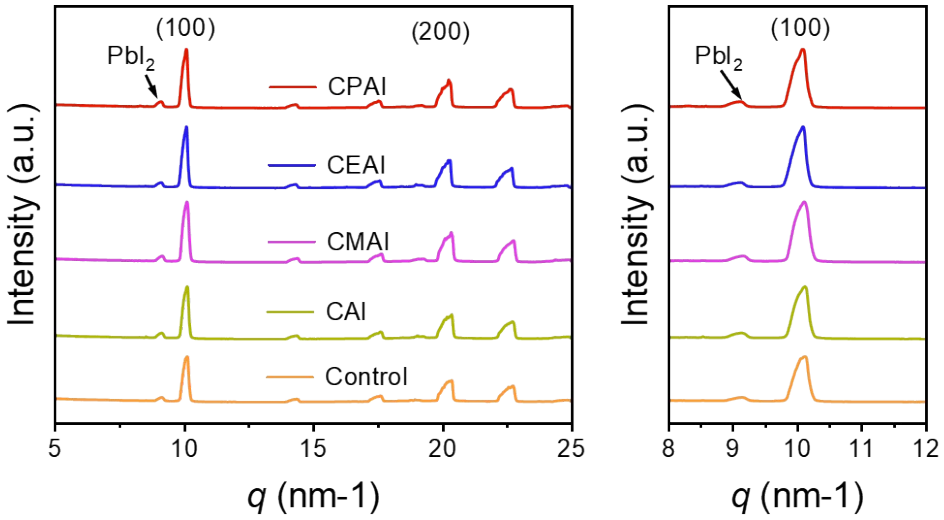

Fig. S10 Radially integrated curves of the control and passivated perovskite films.

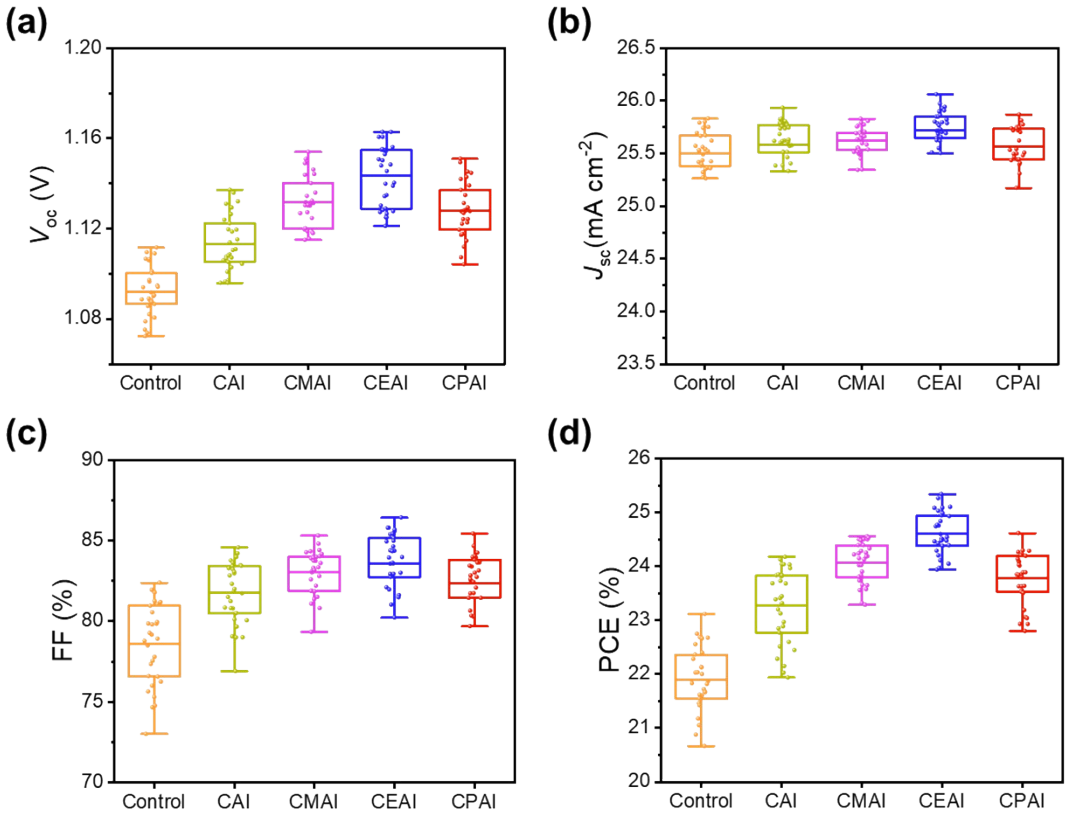

Fig. S11 Device statistics for (a) V_{OC}, (b) J_{SC}, (c) FF, and (d) PCE with different surface modifications.

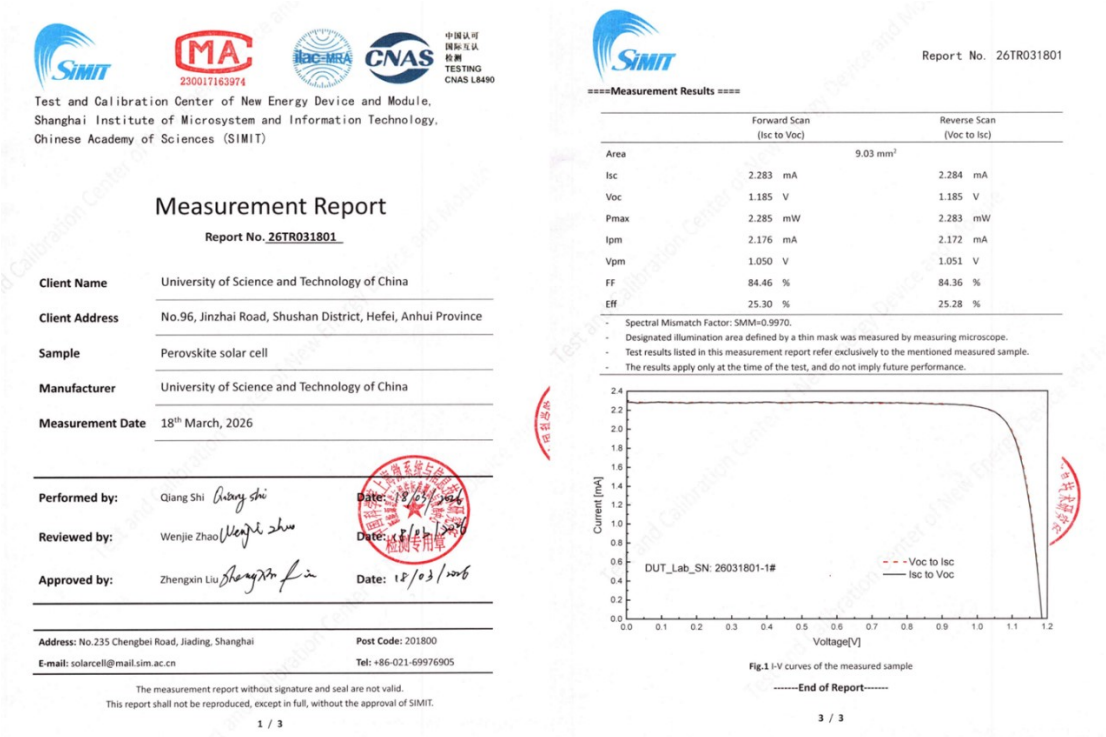

Test and Calibration Center of New Energy Device and Module,
Shanghai Institute of Microsystem and Information Technology,
Chinese Academy of Sciences (SIMIT)

Measurement Report

Report No. 26TR031801

Client Name	University of Science and Technology of China
Client Address	No.96, Jinzhai Road, Shushan District, Hefei, Anhui Province
Sample	Perovskite solar cell
Manufacturer	University of Science and Technology of China
Measurement Date	18th March, 2026

Performed by: Qiang Shi Date: 18/03/2026
Reviewed by: Wenjie Zhao Date: 18/3/2026
Approved by: Zhengxin Liu Date: 18/03/2026

Address: No.235 Chengbei Road, Jiading, Shanghai Post Code: 201800
E-mail: solarcell@mail.sim.ac.cn Tel: +86-021-69976905

The measurement report without signature and seal are not valid.
This report shall not be reproduced, except in full, without the approval of SIMIT.

1 / 3

Report No. 26TR031801

====Measurement Results ====

	Forward Scan (Isc to Voc)	Reverse Scan (Voc to Isc)
Area	9.03 mm²	
Isc	2.283 mA	2.284 mA
Voc	1.185 V	1.185 V
Pmax	2.285 mW	2.283 mW
Ipm	2.176 mA	2.172 mA
Vpm	1.050 V	1.051 V
FF	84.46 %	84.36 %
Eff	25.30 %	25.28 %

- Spectral Mismatch Factor: SMM=0.9970.
- Designated illumination area defined by a thin mask was measured by measuring microscope.
- Test results listed in this measurement report refer exclusively to the mentioned measured sample.
- The results apply only at the time of the test, and do not imply future performance.

Fig.1 I-V curves of the measured sample

-------End of Report-------

3 / 3

Fig. S12 The certified performance of the target device measured at SIMIT. The device exhibits a certified PCE of 25.30% (under forward scan) and 25.28% (under reverse scan) with negligible hysteresis.

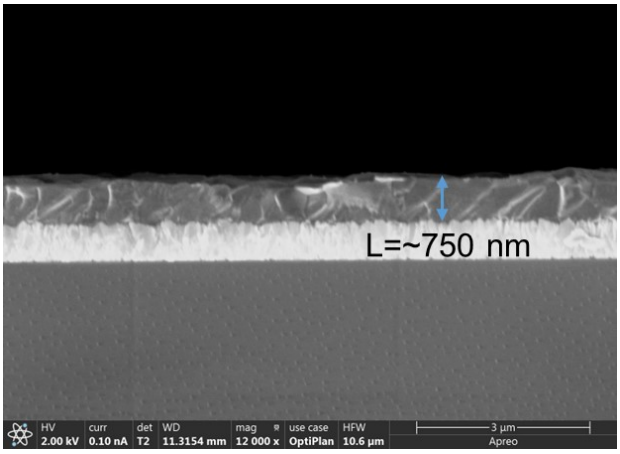

Fig. S13 The cross-sectional SEM image of $FAPbI_3$ perovskite film.

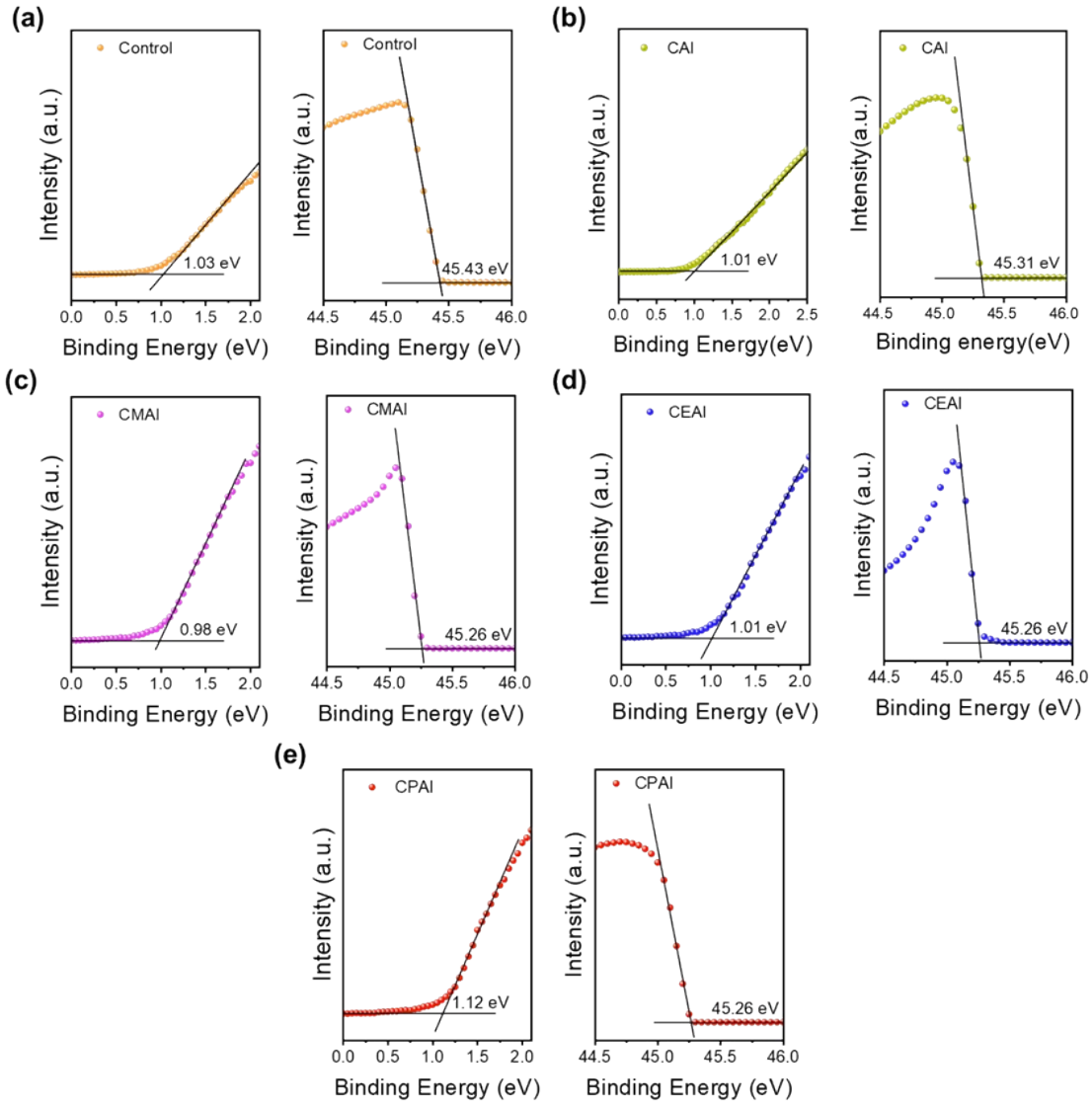

Fig. S14 UPS spectra comparing surface-modified perovskite films: (a) Untreated (control), (b) CMAI treatment, (c) CMAI treatment, (d) CEAI treatment, (e) CPAI treatment. Ultraviolet photoelectron spectroscopy (UPS) is usually employed to determine the energy band structure of perovskite films with respect to the vacuum level (E_{VAC} = 0 eV). The work function (WF) was calculated by WF = $h\nu - E_{cutoff}$ from the secondary electron threshold, where the excitation photon energy ($h\nu$) is 50 eV. The valence band maximum is found by a linear extrapolation of the leading edge of the Fermi edge of the spectra. The valence band (E_V) is calculated by E_V = (WF + E_{onset}). Accordingly, we further calculated the conduction band energy level (E_C) by $E_C = E_V + Eg$ (band gap of the perovskite), where band gaps are extracted from the optical

absorption spectrum (Fig. S15) via a Tauc Plot method in which extending the section of the straight line of the curve to the x-axis and the intercept of the line gives the optical band gap. The binding energy (E_b) is converted by $E_b = h\nu$ − WF $(Instrument) - V_{bi} - E_k$, where the work function of the instrument is 4.3 eV, the applied bias to the sample V_{bi} is -5 V, E_k is the kinetic energy measured directly by the instrument. The related parameters were summarized in Table S8.

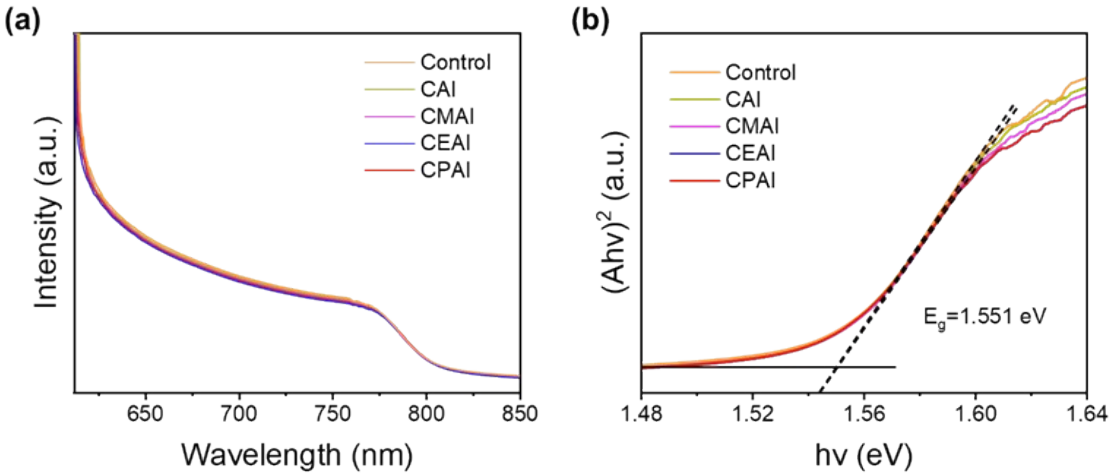

Fig. S15 (a) The optical absorption spectra and (b) Tauc plots of control and passivated perovskite films.

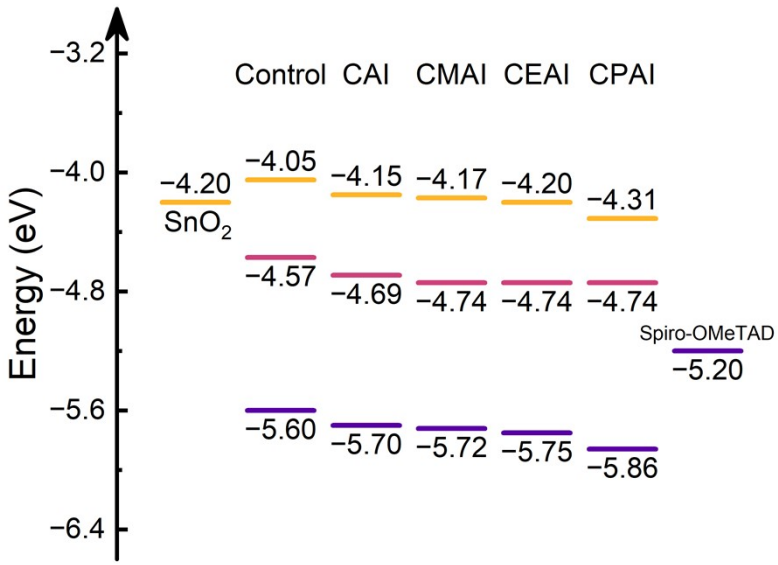

Fig. S16 Energy-level diagram for control and passivated $FAPbI_3$ perovskite films based on the parameters derived from UPS spectra.

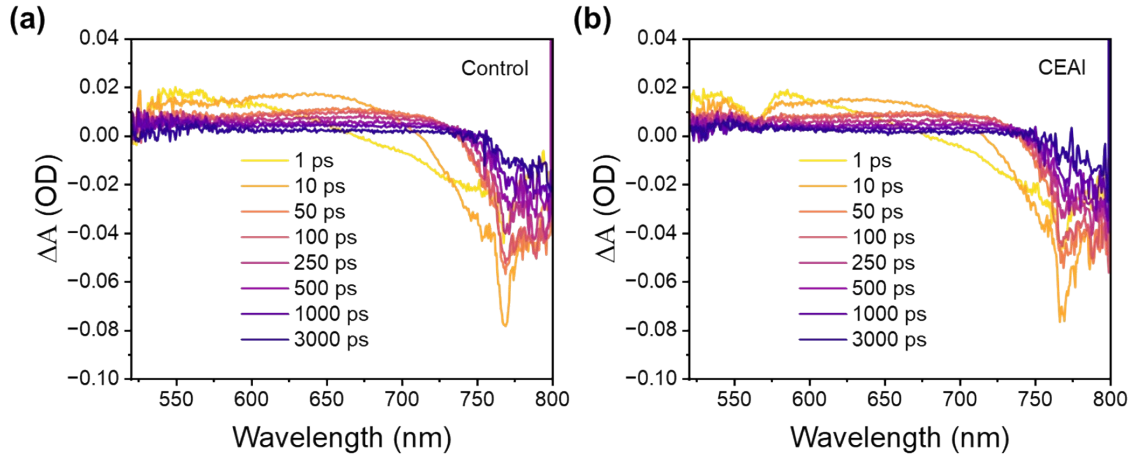

Fig. S17 TAS of control and CEAI-passivated films excited at 400 nm.

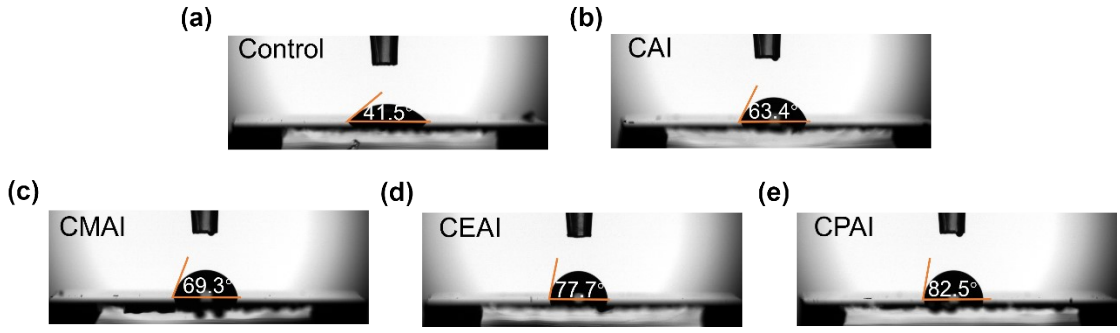

Fig. S18 Water contacts angles of the different perovskite films. (a) Control, and (b-e) with different passivation molecules treatment.

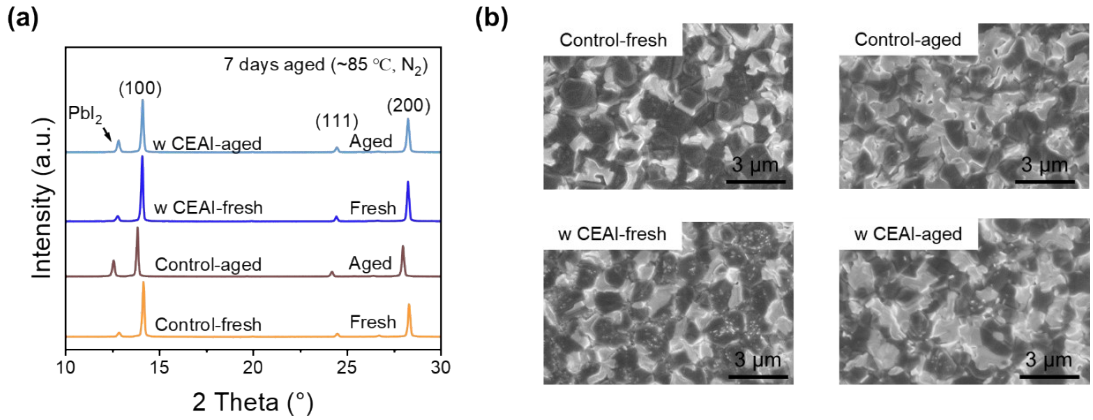

Fig. S19 (a) XRD and (b) Top-view SEM images of the perovskite films without (control) and with CEAI passivated after 7 days of thermal aging, respectively (temperature: 85 °C; in the N_2 glove box).

Table S1. Fitted parameters of the time-resolved PL spectra for control and passivated perovskite films.

Devices	A_1	τ_1 (ns)	A_2	τ_2 (ns)	τ_{ave} (ns)
Control	0.52	73.0	0.44	404.3	346.0
CAI	0.59	56.1	0.37	333.5	274.8
CMAI	0.94	43.5	0.24	279.2	189.9
CEAI	0.75	38.9	0.27	240.6	178.1
CPAI	0.89	42.8	0.25	272.1	189.4

The results are obtained by using the double exponential equation (Eq. S1) to fit the time-resolved PL spectra and τ_{ave} is calculated according to the Eq. S2.

$$f(t) = A_1\exp(-\frac{t}{\tau_1}) + A_2\exp(-\frac{t}{\tau_2}) + B \quad \text{(S1)}$$

$$\tau_{ave} = \frac{A_1\tau_1^2 + A_2\tau_2^2}{A_1\tau_1 + A_2\tau_2} \quad \text{(S2)}$$

Table S2. The photovoltaic parameters of control and passivated perovskite devices.

Average[a]	V_{oc} (V)	J_{sc} (mA/cm^{-2})	FF (%)	PCE (%)
Control	1.092±0.011	25.51±0.24	78.58±2.54	21.89±0.60
CAI	1.113±0.012	25.58±0.36	81.72±1.90	23.26±0.68
CMAI	1.132±0.011	25.62±0.12	83.00±1.35	24.07±0.40
CEAI	1.144±0.013	25.72±0.25	83.60±2.08	24.60±0.36
CPAI	1.128±0.012	25.57±0.17	82.34±2.21	23.78±0.48

[a] Averaged 30 devices fabricated independently.

Table S3. The photovoltaic parameters for different concentrations of CAI-passivated perovskite devices.

Concentration (mM)	V_{OC} (V)	J_{SC} (mA/cm^{-2})	FF (%)	PCE (%)
0	1.092±0.011	25.51±0.24	78.58±2.54	21.89±0.60
5	1.091±0.023	25.57±0.12	80.03±2.73	22.32±0.46
10	1.113±0.012	25.58±0.36	81.72±1.90	23.26±0.68
15	1.110±0.020	25.65±0.29	81.17±2.65	23.11±0.56

Table S4. The photovoltaic parameters for different concentrations of CMAI-passivated perovskite devices.

Concentration (mM)	V_{OC} (V)	J_{SC} (mA/cm^{-2})	FF (%)	PCE (%)
0	1.092±0.011	25.51±0.24	78.58±2.54	21.89±0.60
5	1.119±0.013	25.62±0.11	82.19±3.53	23.56±0.46
10	1.132±0.011	25.62±0.12	83.00±1.35	24.07±0.40
15	1.126±0.020	25.58±0.20	82.87±2.15	23.87±0.38

Table S5. The photovoltaic parameters for different concentrations of CEAI-passivated perovskite devices.

Concentration (mM)	V_{OC} (V)	J_{SC} (mA/cm^{-2})	FF (%)	PCE (%)
0	1.092±0.011	25.51±0.24	78.58±2.54	21.89±0.60
5	1.125±0.019	25.60±0.31	82.32±1.73	23.70±0.44
10	1.144±0.013	25.72±0.25	83.60±2.08	24.60±0.36
15	1.136±0.011	25.55±0.29	82.86±1.99	24.04±0.28

Table S6. The photovoltaic parameters for different concentrations of CPAI-passivated perovskite devices.

Concentration (mM)	V_{OC} (V)	J_{SC} (mA/cm^{-2})	FF (%)	PCE (%)
0	1.092±0.011	25.51±0.24	78.58±2.54	21.89±0.60
5	1.117±0.023	25.49±0.37	80.92±1.52	23.03±0.44
10	1.128±0.012	25.57±0.17	82.34±2.21	23.78±0.48
15	1.126±0.018	25.58±0.25	82.05±2.19	23.63±0.37

Table S7. Detailed photovoltaic parameters from reverse/forward *J-V* scans of champion devices based on control and CEAI-passivated perovskite films.

Devices	Scan direction	V_{OC} (V)	J_{SC} (mA cm^{-2})	FF (%)	PCE (%)	HI[a] (%)
Control	Reverse	1.114	25.58	81.12	23.11	4.67
	Forward	1.103	25.54	78.23	22.03	
w CEAI	Reverse	1.165	25.80	85.13	25.58	1.80
	Forward	1.148	25.78	84.85	25.11	

[a] HI: hysteresis index. HI = ($PCE_{Reverse}$ - $PCE_{Forward}$)/$PCE_{Reverse}$

Table S8. Detailed parameters calculated from the UPS and optical absorption spectrum of control and passivated perovskite films.

Devices	E_F (eV)	WF (eV)	E_{onset} (eV)	E_g (eV)	E_V (eV)
Control	-4.57	4.57	1.03	-4.05	-5.60
CAI	-4.69	4.69	1.01	-4.15	-5.70
CMAI	-4.74	4.74	0.98	-4.17	-5.72
CEAI	-4.74	4.74	1.01	-4.20	-5.75
CPAI	-4.74	4.74	1.12	-4.31	-5.86

Table S9. Transient absorption results of glass/perovskite/Spiro-OMeTAD at 770 nm.

Device	A_1	τ_1 (ns)	A_2	τ_2 (ns)	τ_{ave} (ns)
Control	0.39	13.3	0.59	441.5	433.1
w CEAI	0.56	10.2	0.54	395.3	385.2

Table S10. Parameters employed for the fitting of the impedance spectra for the devices without and with CEAI treatment.

Devices	R_s (Ω)	R_{ct} (Ω)	CPE-T (F)	CPE-P (F)
Control	21.03	6699	3.35E-8	0.93
w CEAI	11.05	2682	1.88E-8	0.96

References

1. G. Kresse and J. Furthmüller, *Phys. Rev. B,* 1996, **54**, 11169–11186.

2. P. E. Blöchl, *Phys. Rev. B,* 1994, **50**, 17953–17979.

3. G. Kresse and D. Joubert, *Phys. Rev. B,* 1999, **59**, 1758–1775.

4. J. P. Perdew, K. Burke and M. Ernzerhof, *Phys. Rev. Lett.,* 1996, **77**, 3865–3868.

5. K. Lee, É. D. Murray, L. Kong, B. I. Lundqvist and D. C. Langreth, *Phys. Rev. B,* 2010, **82**, 81101.